https://doi.org/10.1016/j.conbuildmat.2019.117933

Assessing the Quality of Concrete – Reinforcement Interface in Self Compacting Concrete

Antonios Kanellopoulos [a*], Pericles Savva [b], Michael F. Petrou [b], Ioannis Ioannou [b] and Stavroula Pantazopoulou [c]

[a] *University of Hertfordshire – School of Engineering and Computer Science, College Lane Campus, Hatfield, UK.*

[b] *University of Cyprus - Department of Civil and Environmental Engineering, 75 Kallipoleos Av., P.O. Box 20537, 1678 Nicosia, Cyprus*

[c] *York University – Department of Civil Engineering – Toronto, Ontario, Canada*

Abstract: Research has shown that even self-compacting concrete (SCC) mixtures can exhibit the so-called "top-bar effect" which impacts bond and anchorage. Several instances of conflicting results have nevertheless been published regarding interfacial bond between self-compacting concrete and steel reinforcement. The scope of this paper is to present an experimental methodology for assessing the quality of the interface between self-compacting concrete and ribbed reinforcement. For this purpose, seven different self-compacting and four normally vibrated concrete (NVC) mixtures with diverse rheological characteristics were examined. Digital Image Analysis of cut sections containing reinforcing bars at different cast-heights was used as a diagnostic tool. The study illustrates that the quality of the interface is strongly affected by the viscosity of the SCC mixtures and by the slump values in NVC. Self-compacting concrete mixtures show greater inherent robustness and cohesion at the steel-concrete interface compared to conventionally vibrated concretes.

Keywords: Self Compacting Concrete; top-bar effect; reinforcement-concrete interface; concrete quality

E-mail addresses: ak17acu@herts.ac.uk (A. Kanellopoulos), periclesasavva@gmail.com (P. Savva), petrou@ucy.ac.cy (M. F. Petrou), ioannis@ucy.ac.cy (I.Ioannou), pantazo@yorku.ca (S.Pantazopoulou)

1. Introduction

Reinforcing steel secures strength and ductility to reinforced concrete structures through bonding to concrete, provided that the two materials are in contact through adhesion and interlock. In a similar fashion to the Interfacial Transition Zone (ITZ) concept, the thin zone of cementitious matrix that surrounds the reinforcement plays a dominant role on the reinforcement's bond to the surrounding matrix. In fact, interlocking goes as deep as the bar ribs, to the extent that bars of smaller diameter with smaller size ribs are more susceptible to the so-called top-bar effect [1]. Bleeding water and air migrate towards the surface of the element as the heavier particles settle and get trapped under obstacles encountered in this journey. A primary example of such obstacles are the horizontally embedded reinforcement bars. Besides surface laitance, bleed water and air when trapped will give rise to cavitation. This will lead to high localized porosity, which has undesirable consequences such as high plastic settlement and poor mechanical interlock between the steel reinforcement and concrete.

It is, therefore, critical that the layer of the matrix surrounding the top-cast bars is free of defects and flaws. Among the various types of defects that may develop at the bar-concrete interface, two types seem to be particularly related to the quality of concrete and may occur at the extremes of two possible states: in the case of highly flowable concrete, segregation of the heavier particles may cause highly porous and weak cover, whereas in the other extreme case, that of concrete with very low workability, air voids in the form of micro-honeycombing form under the bar adversely affecting the interfacial bond [1–9]. In engineering practice, the quality of interface is usually studied through standard pull-out bond tests [1-3]. This is highly time consuming and very slow at yielding results as it requires maturity of concrete (28 days). In the present study an alternative diagnostic tool is considered: the condition of the interface is studied through digital image analysis with reference to large voids and local pore distribution, and the result is correlated with important mix variables that may be used as predictors of the quality of the achieved interlock. To cover the range of concrete flowability behaviour, two types of concrete mixes are used in the study for corroboration of measured interface condition and mix characteristics: (a) Self-compacting concrete

(SCC) mixes with similar mix design but different viscosities, (b) Normal vibrated concretes (NVC) having different workability.

1.1 Parameters Influencing the Interface Properties

SCC is a major advance in the construction industry as it is highly flowable and consolidates under its own weight, thereby eliminating the need for mechanical vibration during casting [10–13]. In its fresh state, SCC consists of a continuously changing dispersion of cement paste and aggregates. As any other concrete with increased viscosity, many SCCs exhibit a degree of bleeding [14–16].

Increasing the height (thickness) of a concrete element leads to increased risk of bleeding and segregation [10], especially for superplasticized concrete mixtures with increased workability (slump > 150mm). Since such concretes are mainly used in the manufacture of load-bearing deep horizontal structural elements, the issue is of vital importance [17]. An increased likelihood of bleeding consequently affects the quality of the interface between top-cast bars and surrounding concrete and results in inadequate bond performance as compared to bars placed at the bottom of deep structural elements. Thus, the vertical gradation in interface properties between concrete and horizontally anchored reinforcement bars, known as top-bar effect, is a concern in both self-compacting and normally vibrated concretes (NVCs) [1–5, 18].

ACI 318 (2014) associates the top-bar effect with any steel reinforcement that has more than 305 mm of concrete cast below [19]. Similarly, Eurocode-2 (Clause 5.2.2.1, [17]) assumes unfavorable bond due to deficiency at the interface for any horizontally laid bars that lie in the top half of a member (when members are at least 250 mm thick) or in the upper 300 mm of the total member thickness, whichever is less. Note that although the experimental literature on reinforcement to concrete bond is extensive, considerably less data is available regarding the top-bar effect and its correlation to the mixture properties in both NVC and SCC. Note that SCC was developed with the intent to improve the degree and quality of compaction over that of NVC, where compactability is ensured through mechanical vibration. In this context, it would be

expected that SCC may have significantly improved mechanical properties, durability and bond between its matrix and ribbed steel reinforcement. However, there are discrepancies in the published literature, not only concerning the numerical values, but also regarding the associated physicochemical mechanisms responsible for the results. Some researchers show that SCC, being a more cohesive material with a better degree of compaction, exhibits better bond to reinforcement than NVC [3, 4, 6, 8], whereas others report no significant differences [16]. There is also evidence that even SCCs with increased flowability show inadequate bond to top reinforcement [12, 15, 16]. It has therefore been suggested that by altering the concrete mixture viscosity this problem can be addressed [14, 20]. This hypothesis is tested in the present paper through digital image analysis of the concrete-steel interface.

1.2 Steel-concrete interface

Mechanically-vibrated cement-based composites are characterized by the existence of several interfaces in their matrix, the most prevalent being the cement gel-aggregate ITZ. The microstructure of cement paste in the vicinity of an aggregate embedded in mortar (or concrete) differs significantly from the microstructure of cement paste away from aggregates, since particle bonds grow only unilaterally from the gel mass to the aggregate. Furthermore, the concentration of water around the aggregates leads to a higher water-to-cement (w/c) ratio near the interface than in the bulk of the gel. This results in the formation of a more porous matrix in the ITZ. It has been shown experimentally that the ITZ characteristics strongly affect the physico-mechanical properties of NVC [21–23]. In SCC, there is some experimental evidence showing that the ITZ is denser, stronger and wider [21]. The same process governs the formation of the interface zone around embedded reinforcement [24]. Studies on SCC and NVC show that for both types of concrete, the interfacial zone underneath the steel reinforcement is weaker than the corresponding zone above it [7], although this difference is more pronounced in NVC.

Interface defects in the form of macropores which occur in the extreme case of poor workability are another consequence of mix design that is frequently neglected [25]. Macropores represent air voids trapped in the matrix during the processes of mixing, concreting and consolidating. The size of these pores varies from 30 to 200 μm [22, 26].

The performed analysis highlights the relation of the workability of the mixes with the formed porosity and/or cavitation underneath the embedded reinforcement. It also provides the opportunity to have a visual appreciation of the interface between the two materials (concrete and steel) rather than providing a "bond strength" value. The scope of the method hereby proposed is to identify and study the existence and extent of macropores, which not only form the upper limit of capillary pores, but also strongly affect the mechanical properties of the end-product. Using image analysis, an attempt is made to link the characteristics of the mixture to the state of the steel-concrete interface. Smaller capillary (10 nm to 30μm) and inter-layer pores (<10 nm) are not dealt with in the discussion, not only because they cannot be easily depicted by image analysis due to their size, but also because they do not influence the mechanical properties of concrete mixtures to any significant extent [27]. Such pores do not cause significant disconnection between reinforcement bars and surrounding concretes, therefore their effect is not reflected locally at the quality of interface but globally in the magnitude of the material strength. Bond and development capacity depend on the mechanical stresses developed at the reinforcement ribs that interlock in the concrete. Voids at the interface eliminates partially the interlocking action of the ribs with concrete, and as the voids are randomly spaced along the interface, this type of bond deprecation is random. The effect overall on bond is similar to the familiar top bar effect seen in conventional concrete where the concrete is porous around the bar owing to local concentration of water and an increase in the effective water to cement ratio.

2. Materials and specimen preparation

2.1 Mixing and casting of specimens

The concrete mixtures presented in this study were prepared with standard CEM-II 42.5R cement. Eleven mixtures were prepared in total; seven of those were SCC and four NVC. Each of the mixtures represented a different workability/ flowability category. The idea for this is to explore a wide spectrum of viscosities and their effect on the reinforcement/concrete interface. For the production of both types of concrete, graded crushed calcareous coarse aggregates (8-20 mm and 4-10 mm) were used, as well as two different gradings of crushed calcareous sand (0-4 mm and 0-2 mm). Last generation polycarboxylate water-reducing agent (PCWRA) was used for the SCCs, whereas polynaphthalene-based superplasticiser (PNSP) was used for the NVCs. Fine limestone powder with a specific gravity of 2.80 was used in the production of all SCC mixtures. In addition, the effect of the addition of silica fume (94% SiO2) to SCCs was also investigated. All mixtures were designed in such a way as to provide a wide spectrum of rheological properties and meet the spread criteria for being characterised as self-compacting (500 mm < spread < 800 mm). Tables 1 and 2 summarize the mix designs for all the mixtures considered in this work.

Table 1: Mix design characteristics for the self-compacting concrete mixtures. All quantities in kg unless otherwise stated.

	SCC-1	SCC-2	SCC-3	SCC-4	SCC-5	SCC-6	SCC-7
CEM II 42.5R	350	350	350	350	333	313	301
Water	210	175	175	157	175	175	175
Limestone	175	175	175	175	175	175	175
Silica Fume	-	-	-	-	17	37	49
Coarse 8/20	300	300	300	300	300	300	300
Coarse 4/10	500	500	500	500	500	500	500
Sand 0/4	280	280	280	280	280	280	280
Sand 0/2	491	491	491	491	491	491	491
PCWRA (ltr)	6.1	6.5	7.2	13	8.0	8.0	9.3
w/b	0.60	0.50	0.50	0.45	0.50	0.50	0.50

Table 2: Mix design characteristics for the normally vibrated concrete mixtures. All quantities in kg unless otherwise stated.

	NVC-1	NVC-2	NVC-3	NVC-4
CEM II 42.5R	400	400	400	400
Water	200	200	200	200
Coarse 8/20	680	680	680	680
Coarse 4/10	275	275	275	275
Sand 0/4	560	560	560	560
Sand 0/2	110	110	110	110
PNSP (ltr)	-	1.9	3.3	6.4
w/b	0.5	0.5	0.5	0.5

A high shear concrete mixer was used for the production of all concrete mixtures. Consolidation of NVCs was performed with an electric motor vibrating table. From each mixture, ten cubic (100x100x100 mm), one cylindrical (Ø150x300 mm) and two prismatic (100x100x500 mm) specimens were cast for the evaluation of compressive strength, modulus of elasticity and flexural strength respectively.

Moreover, six columns were cast from each mixture. These columns had a square cross-section of 100x100 mm and a height of 600 mm. In three of these columns steel reinforcement bars, with nominal diameter of 12 mm, were embedded at three different locations; the bottom, the middle and the top of the columns (Fig. 1). The steel reinforcement had a cover of 50 mm from both top and bottom surfaces. The purpose of this was to microscopically investigate the interface between the steel bar and the surrounding cementitious matrix. The remaining columns were cast without any reinforcement. These elements were used to identify the compressive strength variation along the height of the specimen.

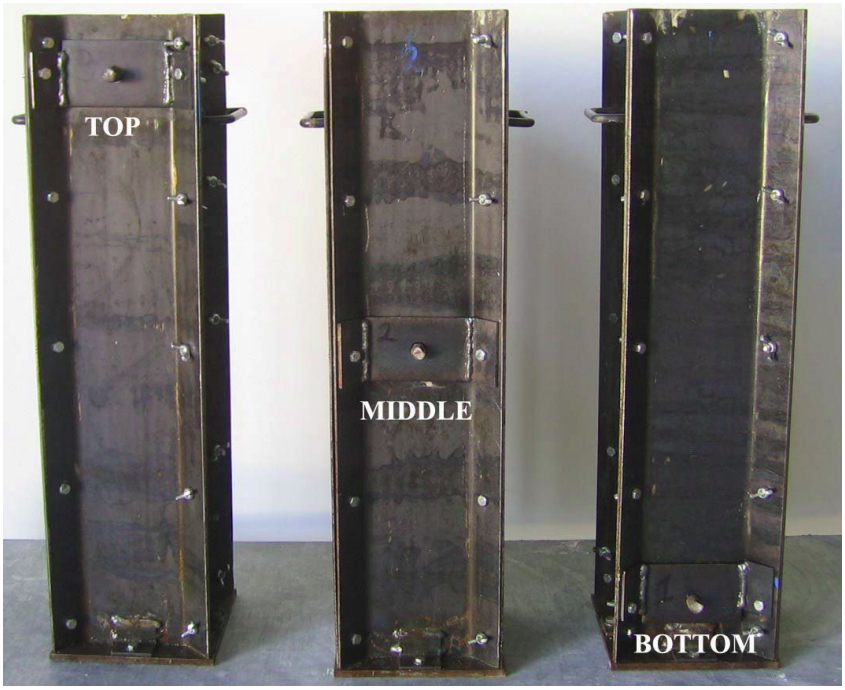

Fig. 1: Non-absorbent metallic column moulds with steel reinforcements at different heights.

All SCC specimens were cast in a continuous manner, whereas the NVC samples were cast in three layers, which were compacted with the aid of an electric vibrating compaction table operating at a constant frequency of 50 Hz. Since the NVC mix designs considered in this study had different workabilities (see Table 3, section 4.1), for consistency purposes these specimens were compacted at the same intensity until macroscopic evidence of adequate compaction (e.g. air bubbles on the cast surface). All specimens were left to set for 20 hours before demoulding, after which they were all immersed in a water tank (20 ºC ±1) for 28-days to cure.

2.2 Preparation of samples for image analysis and strength evaluation with height

The column specimens, with and without reinforcement, were sectioned using a diamond blade saw to create the samples needed for the different experimental procedures. The process of sectioning the columns with reinforcement was as follows: cubic specimens (100x100x100 mm) containing the embedded reinforcement bars were extracted from the columns and bisected in the vertical direction diametrically trough the bars, thereby exposing the reinforcement and the concrete surrounding it (along the dashed lines

in Fig. 2, see also Fig. 3). The remaining part of the column specimen was also bisected in the same manner to observe macroscopically the aggregate distribution away from the reinforcement, and to identify possible segregation and/or homogeneity problems. The entire cutting process was carried out with extreme caution, detail and precision to prevent any local damage.

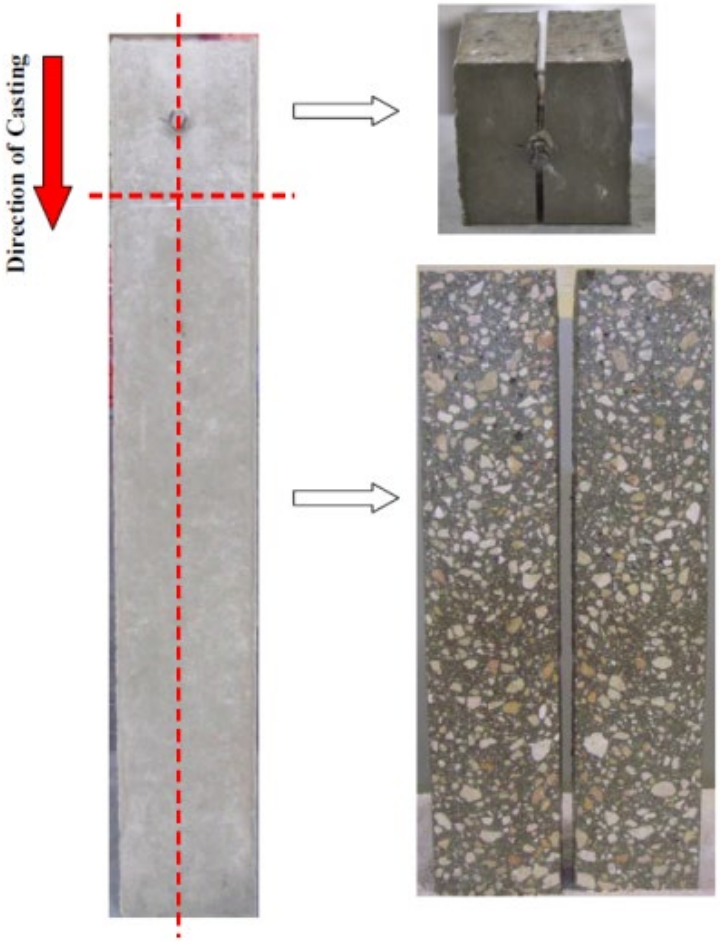

Fig. 2: The sectioning pattern on column-type specimens with reinforcement. Dotted lines indicate the cutting lines followed while bisecting the elements.

Fig. 3: Bisecting of the area around the reinforcement

Each of the columns without any reinforcement was cut into three blocks with a cross-section of 100x100 mm and a height of 200 mm. Two specimens 100x100x100 mm were prepared from each block in order to measure the compressive strength variation along the height of the column (Fig. 4).

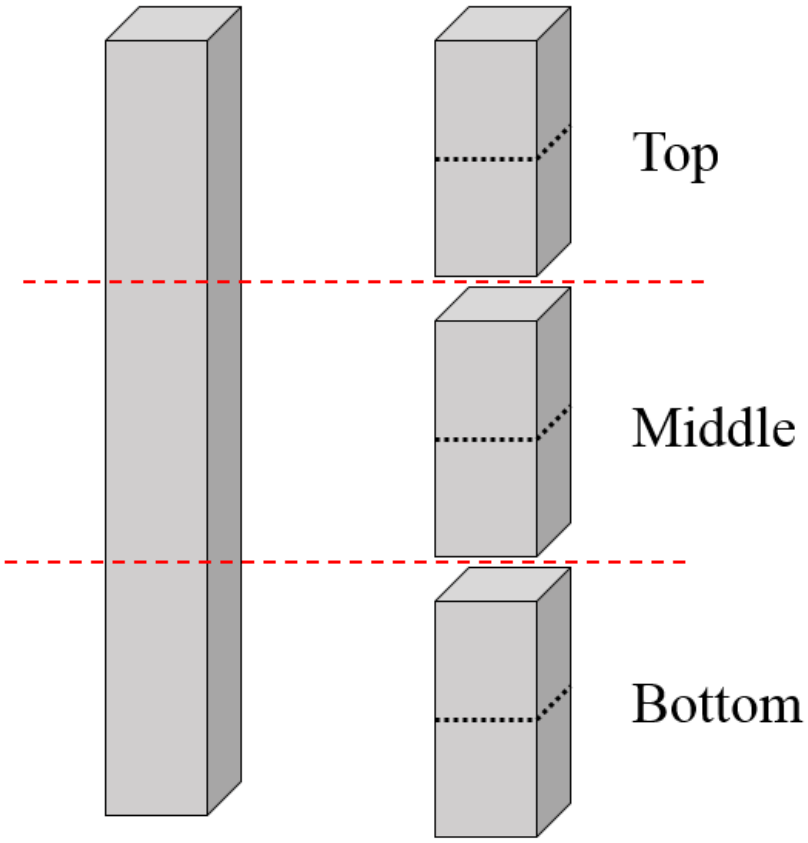

Fig. 4: The sectioning pattern on column-type specimens without reinforcement. Dotted lines indicate the cutting lines followed while cutting the elements.

3. Experimental techniques

3.1 Fresh properties

The workability of the mixtures was assessed with the slump flow-test (SCCs) in accordance with EN 12350-8 [28] and the slump test (NVCs) in accordance with EN 12350-2 [29] Additionally, for SCCs a specially developed rotating rheometer (BT2 Rheometer) was used to obtain relative values of yield stress and plastic viscosity. The classification of the mixtures was done according to the provisions of the European Guidelines for SCC [10, 11].

3.2 Mechanical properties

Compressive strength and modulus of elasticity tests were performed on a 5000 kN servohydraulic compression frame. Flexural strength tests were performed on a 100 kN servohydraulic flexure frame.

3.3 Image analysis

Image analysis is a well-established tool for characterizing the quality of cement-based composites [30–35]. From a stereometric point, porosity is determined based on the area of pores projected on a 2D image [36–38]. In the present study, after sectioning the specimens, the reinforcement bars were removed exposing the interface between the bar and the surrounding concrete. The slices were viewed and photographed digitally in a grey scale mode with the aid of a Leica-EZ4 stereomicroscope at 8x magnification. Since the field of view of the stereoscopic lenses, at the selected magnification level, was small (~15 mm), six to seven images were required in order to cover the full length of each slice. These images were digitally stitched, thus creating an image that showed the full profile of the concrete contact area with reinforcement (Fig. 5). Two such images were created from the complementary half-slices in order to characterize the concrete-reinforcement contact profile for each bar position (bottom-middle-top).

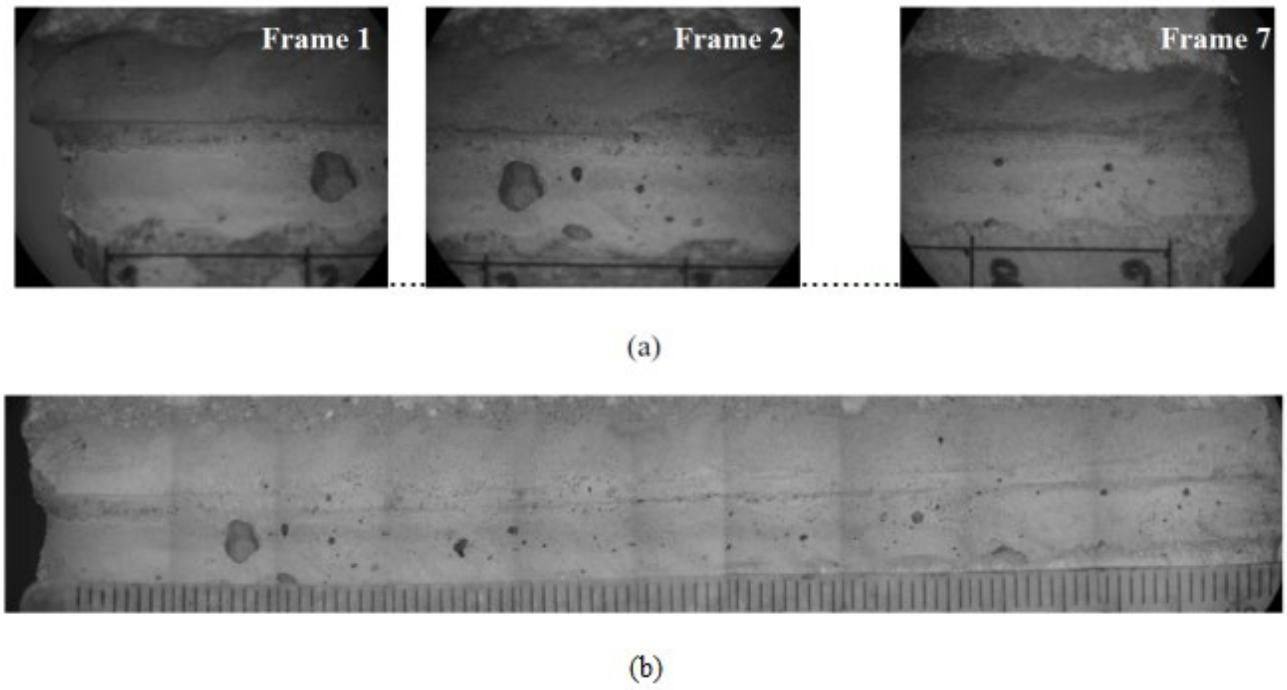

Fig. 5: (a) Selected individually photographed frames; (b) Digitally stitched image containing all frames: the transparent scale at the lower edge of the field of view is used for calibration of the image analysis software; the distance between each black line is 1 mm.

The Image-J freeware package was used for all the image analyses described in this paper. Initially the images, as seen in Fig. 5b, were loaded to the software. Their outer perimeter was cropped to avoid edge effects, resulting in a rectangular image having a total area of 850 mm^2. The grey scale image was then thresholded to differentiate the pore and solid phases, with pores being designated in black and continuously masked and numbered automatically (Fig. 6). The condition of each section defined the strategy required to analyse it. For instance, in the sections containing no visible cavities, the analysis focused on pores, measuring their area and total number. In cases where cavities existed (Fig. 7) the software was used to obtain the total area of cavities as well. The individual pore areas, including cavities, were summed and the result was then divided by the total image area to provide the fraction area of pores.

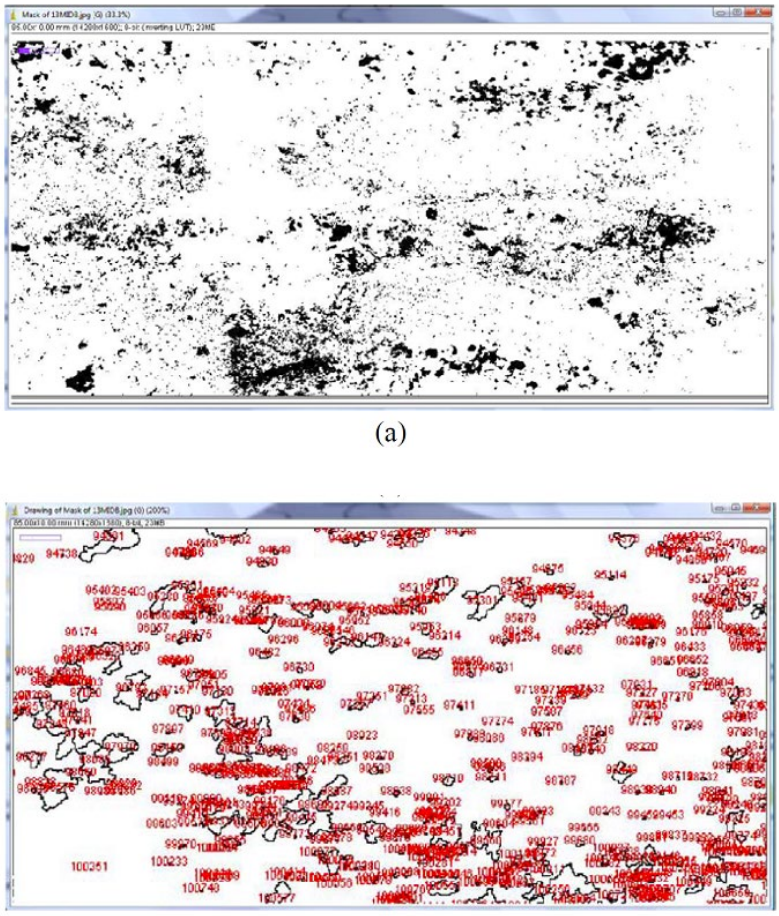

(a)

(b)

Fig. 6: (a) Thresholded image, differentiating solid phase from pores (dark areas); (b) Pores identified and outlined by the software.

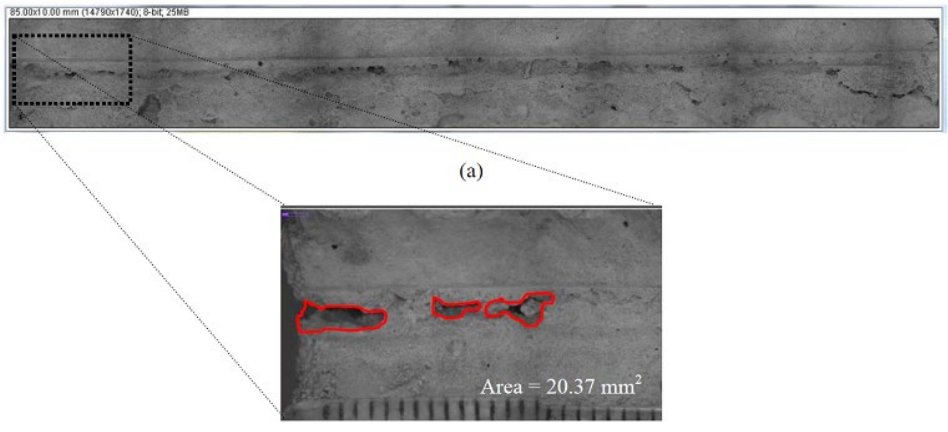

(a)

(b)

Fig. 7: Using the image analysis software to obtain the areas of cavities in cut sections: (a) Identifying the cavities on the section; (b) Magnifying the cavity area and measuring it.

4. Results and discussion

4.1 Fresh properties

Table 3 summarizes the fresh properties for all SCC and NVC mixtures studied in this work.

Table 3: Summary of the fresh properties for all SCC and NVC mixtures.

	SCC-1	SCC-2	SCC-3	SCC-4	SCC-5	SCC-6	SCC-7	NVC-1	NVC-2	NVC-3	NVC-4
w/b	0.60	0.50	0.50	0.45	0.50	0.50	0.50	0.5	0.5	0.5	0.5
Viscosity (N·s)	848.7	4200	1320	3795	885	1470	714	-	-	-	-
Yield stress (Pas)	46	242	43	35	17	60	60	-	-	-	-
Spread (mm)	770	520	782	735	783	725	788	-	-	-	-
Slump (mm)	-	-	-	-	-	-	-	49	114	179	200
Classification	SF3	SF1	SF3	SF2	SF3	SF2	SF3	S2	S3	S4	S4/S5

Note that by reducing the w/b ratio from 0.6 to 0.5 and 0.45 in mixtures SCC-1, SCC-2 and SCC-4, the viscosity was increased by 4 - 5 times, despite doubling the amount of superplasticizer to offset this effect in SCC-4. This is expected since the use of superplasticizer increases flowability without reducing significantly the viscosity [39]. In fact, these three mixtures are at the extreme opposite limits of being characterized as SCCs. They were, therefore, used to identify the quality of steel-concrete interface at extreme mixture conditions. Mixture SCC-3 is a typical good quality SCC, whereas mixtures SCC-5 to 7 showed very good consistency as a result of the use of silica fume. With regards to the NVC mixtures, albeit all four mixtures shared the same basic mix design, they exhibited different slump, because of the different amounts of PNSP used– becoming progressively more workable from NVC-1 to NVC-4. This provided a high range of rheological characteristics in an attempt to identify their effect on the concrete/steel interface.

4.2 Mechanical properties

At the end of the 28-day curing regime, the specimens were removed from the water tank and tested for evaluation of their mechanical properties. Table 4 summarizes the results for all mixtures. The relatively increased water content of the first mixture (SCC-1), as well as its highly flowable nature, resulted in a

material with decreased strength and modulus of elasticity, which did not meet the expected performance requirements for this type of concrete. Note that SCC-1 complied with all requirements for being characterized as self-compacting at the fresh state. Moreover, in macroscopic observation of cut sections, no aggregate settlement or segregation was observed. However, the high water content in SCC-1 affected negatively the mechanical performance of the material. By reducing the water content, the performance of the mixtures improved. The situation was much improved in SCC-2, where the water content was reduced to 0.5; the problem was reversed in SCC-4, where the water content was further reduced, and the self-compacting properties of the mixture were regulated with PCWRA. In fact, the low water-to-binder ratio (w/b) and high viscosity of SCC-4 affected its degree of compaction, thus resulting in lower than expected mechanical properties. SCC mixtures 5, 6 and 7 had improved mechanical properties due to the use of silica fume.

Table 4: Mechanical properties for self-compacting and normally vibrated concretes.

	SCC-1	SCC-2	SCC-3	SCC-4	SCC-5	SCC-6	SCC-7	NVC-1	NVC-2	NVC-3	NVC-4
f_{cu} (MPa)	44	63	63	60	70	75	78	56	58	60	64
f_{cf} (MPa)	5.5	6.0	6.1	8.1	6.0	7.0	7.0	6.4	5.7	5.9	7.0
E (GPa)	26	30	29	29.5	30	32.5	36.7	25	26	26.5	27

NVC mixtures exhibited a more predictable behavior, showing improved mechanical performance with increasing slump (and PNSP amount). Improvement in the workability of the mixture resulted in enhanced compaction, which in turn yielded a denser material with better mechanical response. SCC mixtures (without silica fume) contained less cement (350 kg in SCC vs 400 kg in NVC) but exhibited a better mechanical performance, with the exception of SCC-1, compared to NVCs. This is attributed to the better packing of particles within their microstructure, resulting from the increased amount of fines used.

4.3 Image analysis results

Table 5 shows the results from image analysis of the cut sections. From these results, it is concluded that the two extreme cases of SCC (i.e., the very flowable SCC-1 and the very viscous SCC-2) showed very

weak cohesion between concrete and steel reinforcement at the top part of the element, expressed by the cavity areas. Although the pore fraction percentage is relatively low in both mixtures, the lack of cohesion is manifested by large through-cavities at the bottom half of top reinforcement (Fig. 8).

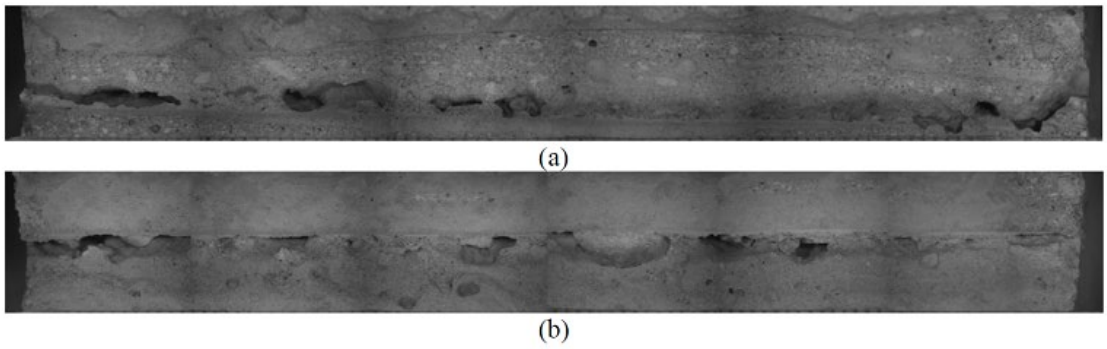

Fig. 8: The two sections of SCC-2 top bar with a visible through cavity.

SCC-1 was the only mixture that exhibited some cavitation in the middle bar as well. The cavity area value in Table 5 concerns the sum of all areas in the cut cross section. However, for SCC-1 the cavity area at the top was three times the corresponding area at the middle of the specimen (approximately 230 mm^2 and 80 mm^2 respectively). Considering that the total area of the cut-section under the lens was 850 mm^2, 27% of the top part of the element was covered by a long continuous crack-like defect. Moreover, for both SCC-1 and SCC-2, a relatively large number of pores was counted. The reason for this lies in the nature of the mixtures. SCC-1 was a highly flowable mixture, which was close to the point of segregation; as a result, excessive amounts of water and air moved upwards causing pore congestion in the microstructure of the material. On the other hand, SCC-2 was a very stiff mixture with relatively high value of plastic viscosity, which rendered the movement of air and water within the material difficult. Hence, the degree of compaction in this mixture was not adequate and indeed was reduced with the height of the element. This was verified by the increasing amount of pore ratio from the bottom to the top of the specimen, whilst it was also evident macroscopically (Fig. 9). In certain occasions cavitation under the reinforcement was even evident with naked eye, by simply observing the surface of the samples.

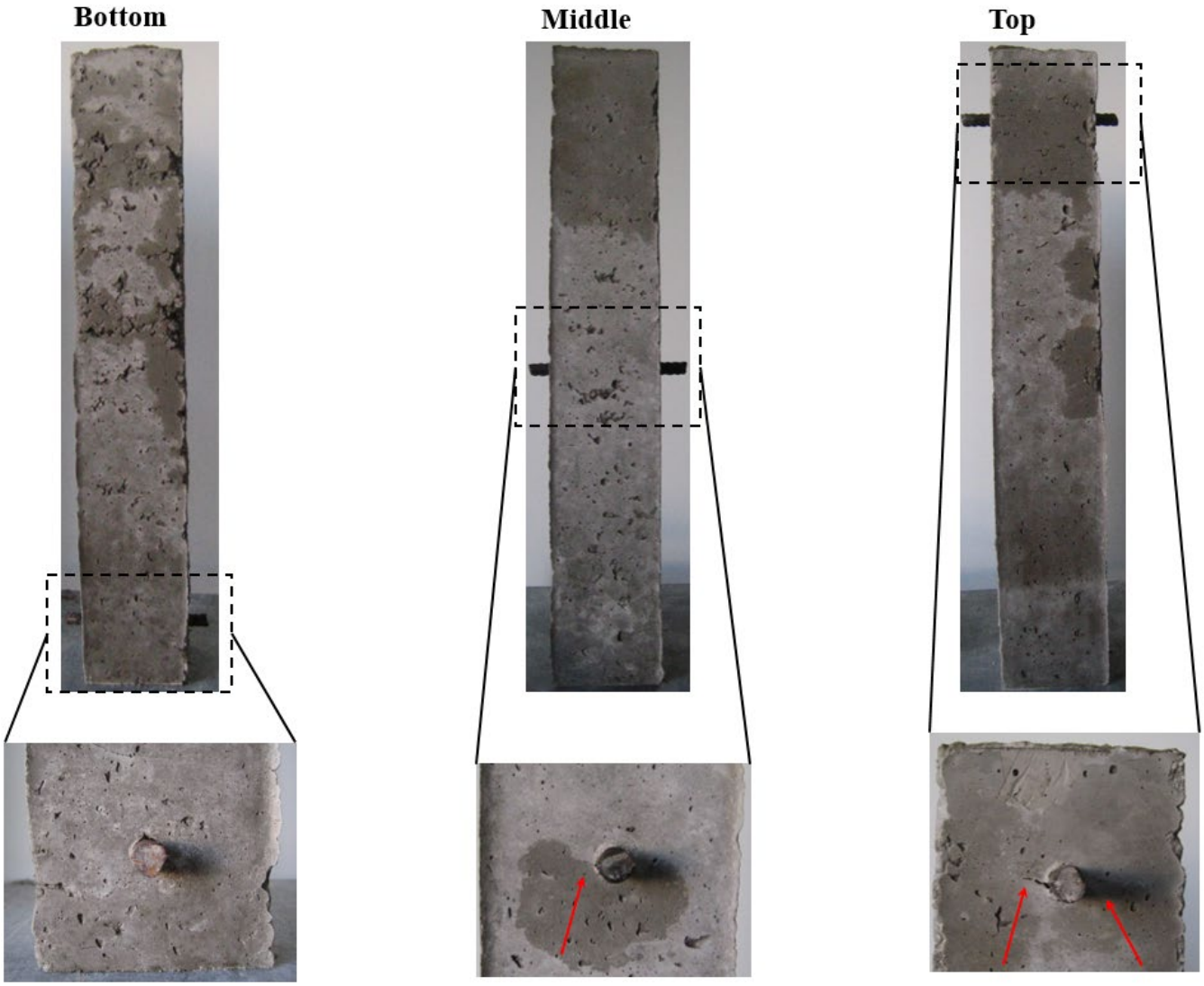

Fig. 9: A typical example of SCC-2 sample. Note the rough nature of the surface, an indication of low levels of self-compaction. Red arrows point to cavitation points, visible on the surface of the samples, appearing as cracks.

Table 5: Image analysis results for pore fraction and total number of pores: (a) for the SCC mixtures and (b) for the NVC mixtures (Note: Cumulative cavity area refers to cavities under all bars).

(a)

		SCC1	SCC2	SCC3	SCC4	SCC5	SCC6	SCC7
	Cumulative Cavity Area (mm^2)	311.9	123.1	-	-	-	-	-
Pores %	TOP	7.2	11.7	6.3	12.9	6.8	9.2	7.4
	MID.	7.3	11.0	7.8	15.7	7.6	11.2	8.7
	BOT.	6.9	9.8	8.4	14.3	7.7	11.1	5.7
Average Pore %		7.1	10.8	7.5	14.3	7.4	10.5	7.3
Pores Counted	TOP	55500	54300	34400	33500	30900	32300	27000
	MID.	60400	72830	37500	73000	41200	39000	36900
	BOT.	60800	88800	38600	65400	48700	42200	25200
Average Pore Count		58900	71977	36833	57300	40267	37833	29700
Pore Diameter (μm)	TOP	41	50	50	58	47	46	50
	MID.	38	44	52	55	48	45	50
	BOT.	36	38	54	55	44	42	50
Average Pore Diameter		38	44	52	56	46	44	50

(b)

		NVC1	NVC2	NVC3	NVC4
	Cumulative Cavity Area (mm^2)	-	20.11	50.2	176.1
Pores %	TOP	11.4	9.6	11.7	7.7
	MID.	-	10.9	10.9	13.6
	BOT.	6.3	11.5	11.5	17.0
Average Pore %		8.8	10.6	11.3	12.8
Pores Counted	TOP	47600	49900	49000	17000
	MID.		45700	57600	18400
	BOT.	38200	56400	60300	22000
Average Pore Count		42900	50667	55633	19133
Pore Diameter (µm)	TOP	54	48	51	79
	MID.	54	40	51	72
	BOT.	51	39	46	57
Average Pore Diameter		53	42	49	69

As mentioned before, SCC-3 represented a good quality and very robust mixture with water-to-binder ratio (w/b) equal to 0.50. In this case, both the pore fraction and total number of pores were lower, compared to the first two mixtures. This particular mixture did not exhibit any significant cavities around the top reinforcement, with the exception of a trapped air pocket, resulting in the value recorded in Table 5. Additionally, it was observed that the top reinforcement exhibited a lower pore fraction and smaller number of pores, compared to the middle and bottom bars, which indicates that no excess amounts of air or water had moved to the top. Reducing the w/b ratio to 0.45 and maintaining the flowability by considerably increasing PCWRA, resulted in a mixture (SCC-4) with a lower degree of compaction. Although the mixture complied sufficiently well with slump flow test requirements, its viscosity was relatively high, making it difficult to handle after a short period of time. The increased cohesiveness of the material had an adverse effect on the degree of compaction and that was verified by the increased pore fraction and number of pores counted. As in the case of SCC-2, the highly viscous nature of the matrix did not allow pores to move freely within its volume, thus resulting in larger pore fraction values at the top reinforcement.

Mixtures SCC-5, SCC-6 and SCC-7 containing silica fume also showed good quality and robustness. With the exception of SCC-5, the other two mixtures showed higher values of pore fraction at the top; however, they had lower overall pore count. More importantly, the inclusion of silica fume, as expected, resulted in the reduction of pore sizes. Silica fume refined the pore network of macropores and reduced their total numbers (especially compared to the less viscous SCCs and all NVCs), thereby increasing the potential for a better mechanical interlock between concrete and reinforcement. From the results for SCC-5 and SCC-7, it was observed that there were no significant differences in the pore fraction. Both SCC-5 and SCC-7 had nearly identical values of plastic viscosity, which were somewhat lower than those of SCC-3. Figure 10 shows the pore fraction variation with viscosity at bottom, middle and top reinforcements for all SCC mixtures.

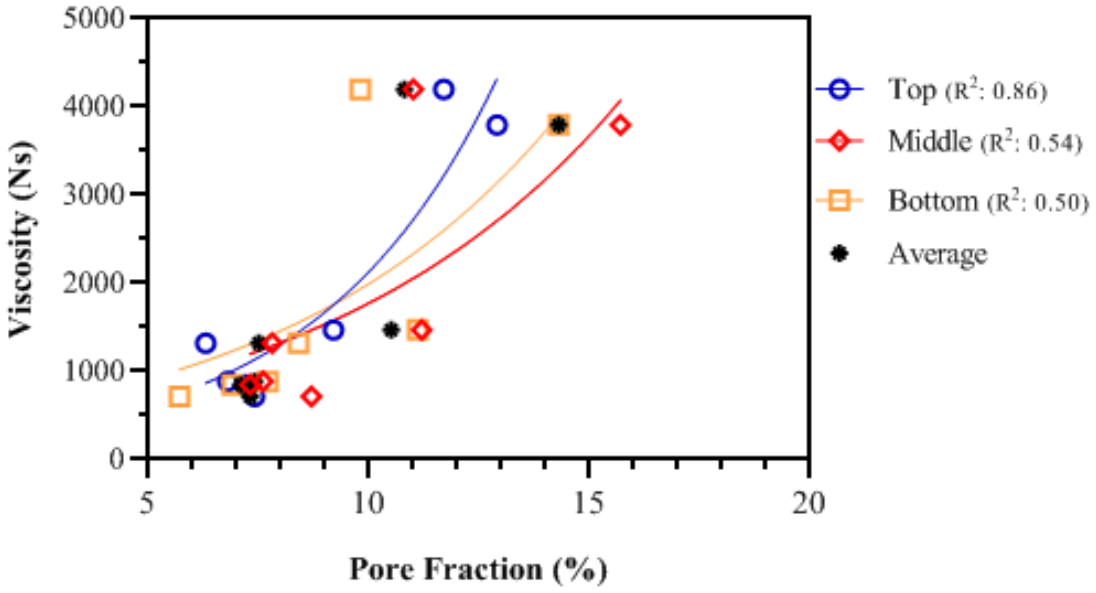

Fig. 10: Pore fraction variation with increasing viscosity for bottom, middle and top reinforcements (SCC mixtures).

The data shows an increase of the measured pore fraction with increasing viscosity and towards the top bar. That is an indication that the top bar locations are indeed very prone to form large pore fractions if the viscosity of the mixture is not optimum. From the obtained data, it appears that mixtures with relative viscosities between 500 Ns to 1500 Ns result in relatively low pore fractions, typically less than 8%. Nonetheless, above the threshold of 1500 Ns, the situation dramatically changes.

Normally vibrated concretes, in general, exhibited greater potential for defective concrete to top-steel interface, compared to the better quality SCCs with the same w/b ratio. This was expressed with larger values of the relevant parameters in all categories of evaluation: pore fraction, pore number and mean pore diameter. In this case, increasing the workability (i.e. reducing yield stress and viscosity) of the mixture resulted in gradually magnifying the problem of macropores' concentration under the bars, and especially at the top section of the specimens. As shown in Table 5, the increase of slump from 49 mm to 200 mm resulted in a gradual increase in the formation of cavities, alongside with the pore fraction and total number of pores. The workability of NVCs, expressed in terms of slump, was inversely proportional to the yield

stress and viscosity of each mixture. High slump mixtures were more flowable and hence had reduced viscosity and vice versa. In the case of NVCs, there is no clear correlation for individual depth location, although the average values show a more distinctive correlation (Fig. 11).

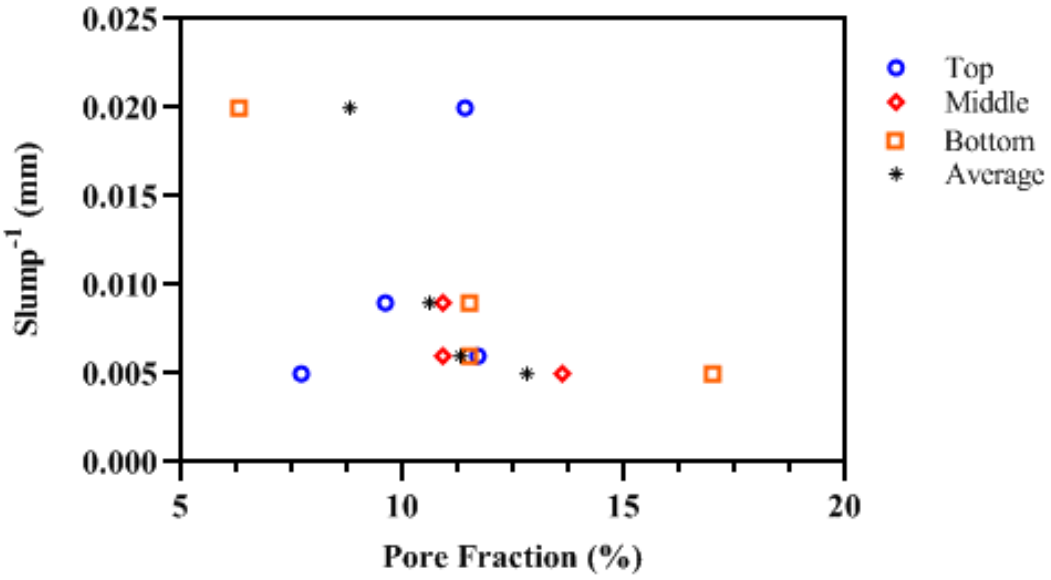

Fig. 11: The variation of the measured pore fraction with the inverse of slump (as an indication of viscosity) for all normally vibrated concrete mixtures.

Note that increasing slump implies reduced viscosity. The situation here is somewhat reversed to what it was observed in SCCs. With increasing slump, hence with reduction of viscosity, the measured pore fractions increase considerably. This finding highlights the sensitivity of low viscosity NVCs to vibration, especially when specific geometries are concerned. Another point that may affect the quality of the interface, especially in SCCs, is the size of cover. Although the selected cover (50 mm) is considered to be typical and in compliance with the diameter of the reinforcing bar used, it might not be large enough for the material to self-consolidate under its own weight at the top of the elements.

Image analysis showed that, in terms of reinforcement cohesion, SCC had a better performance compared to NVCs of the same w/b ratio and workability/flowability class. The viscosity of the mixtures clearly

affected the condition of the concrete-reinforcement interfacial zone. However, the method of reducing viscosity seems to also have an effect. Note that in the series of tests considered, modification of viscosity was effected in three different ways: (a) In SCC-1 to 4, viscosity was modified by varying the w/b ratio and through the addition of PCWRA; (b) in SCC-5 to 7 this was achieved by addition of different amounts of silica fume, whereas (c) in NVC, viscosity was modified by varying the amount of PNSP used. It appears that there is an optimum viscosity value for which requirements for both fresh properties and adequate steel-concrete cohesion are satisfied for SCC mixtures of the same class. For both SCC and NVC mixtures, the quality of interface was significantly compromised, especially at the top side of an element, in very workable/flowable mixtures. This top-bar effect is consistent with observations reported in the literature, which resulted from mechanical testing on bond [12, 23]. At the other end of the spectrum, deficient interface was observed in mixtures with increased degree of cohesiveness, as quantified either by very low spread values (SCC-2) or through reduced flowability due to reduced water content and increased PCWRA amount (SCC-4). Incorporation of silica fume improved the homogeneity of pore distribution along the height of the element, reducing at the same time the size of pores.

In NVC, lack of cohesion manifested itself rather impressively as slump-related workability increased. Here the profound influence of vibration must be recalled in interpreting the experimental data: unlike SCCs, normally vibrated concrete for low slump mixtures showed a relatively good quality at its interface with steel reinforcement. Better compaction is achieved through the mechanical energy applied to the mixture, in the form of vibration, as it reduces locally the frictional forces between particles of the matrix, resulting in the movement of air pockets towards the surface, with the solid particles moving in the opposite direction. In other words, the more workable a mixture, the less external mechanical work is required to compact it and the more sensitive is the resulting concrete-steel interfacial profile to this process of mechanical assisted consolidation. Based on the literature, the settlement velocity of particles is inversely proportional to the viscosity of the mixture [40]. As can be seen (Table 3), this worked nicely for NVC-1 and NVC-2, giving relatively acceptable interface characteristics, with no top cavities and relatively low

pore fractions. Both these mixtures were in acceptable condition in terms of mechanical properties and workability, although their interface quality was still not as good when compared to SCCs. The situation changed dramatically by increasing slump further, with vibration being the factor that controlled not only the mechanical properties of the material but also the quality of the concrete-steel interface. The same had been observed earlier in a study of the strand end-slip measurements in pre-stressed concrete piles [41].

The reduced viscosity of NVC-4 resulted in the development of considerably fewer pores; however, their size was larger and more importantly, excessive cavitation was observed under the top reinforcement. This confirms earlier test results regarding bond strength in high slump concretes [42]. This finding, along with others presented previously in this manuscript, is considered evidence to the validity and proofing of the proposed methodology for assessment of the concrete-steel interface quality through image analysis. The sensitivity of mixtures to vibration should be seriously considered in practice. Although high slump mixtures in shallow specimens show a better degree of compaction and have improved mechanical properties, in deep specimens there is an increased likelihood of poor cohesion between concrete and reinforcement at the top of the element.

It is therefore concluded that the nature of the interface between steel reinforcement and concrete depends greatly on the viscosity and the inherent flowability (SCC) / workability (NVC) of concrete mixtures. Using image analysis, it was observed that both very high and very low viscosity in SCC produces defects at the interface and that an optimal value should be sought to optimize the quality of the bar-concrete interface; this value should be adequate to prevent segregation and bleeding and maintain suspension of solids during self-compaction. On the other hand, in NVCs the yield stress is much higher than the yield stress in SCCs. During the mechanical vibration of NVCs, however, yield stress is significantly reduced, and it is the viscosity that governs the movement to the bottom of the solid particles. Settlement of solid particles causes the movement of water and air pockets in the opposite direction. In high slump concrete, reduced vibration is required but the result is poorer interface due to low viscosity. Thus, the proposed methodology shows that when viscosity values are outside an optimum spectrum (being either high or

low) the pore and cavity fractions around steel reinforcement tend to increase, warning of low-quality interlock between concrete and steel.

The above observations were further supported by the obtained data for the variation of the compressive strength with the height in all specimens (Fig. 12).

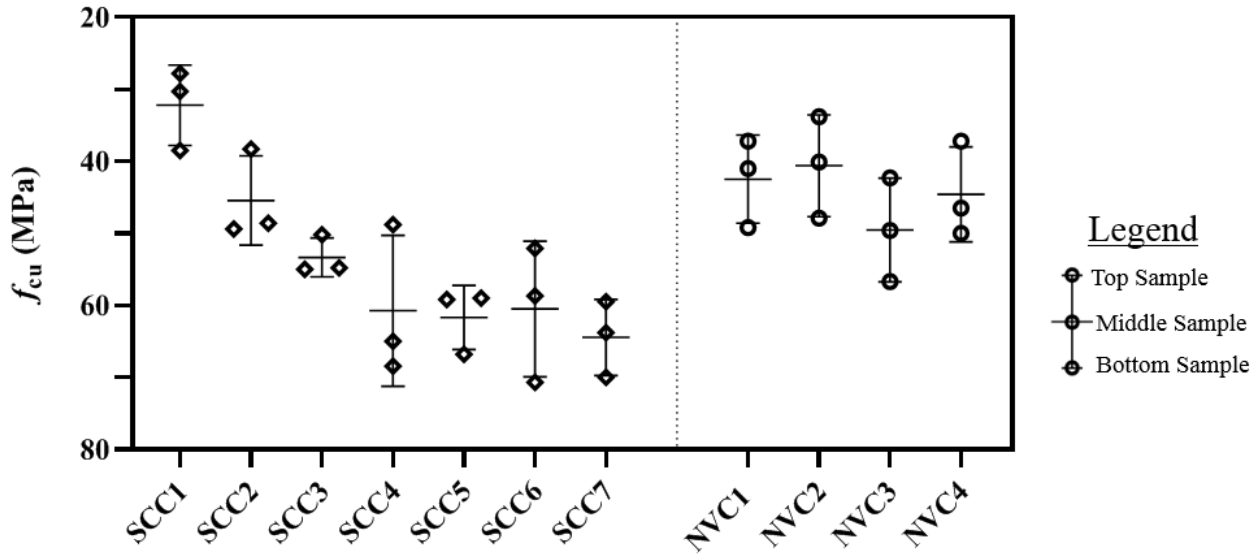

Fig. 12: Variation of compressive strength along the height for all mixtures concerned in this study. Note that y-axis is reversed.

It is evident in all cases that samples from the top of the columns exhibited lower values of compressive strength, which gradually increased towards the bottom of the samples. Regardless the type of the mixture, the bottom half of vertically casted slender specimens is always better compacted than the top half. In some cases, the gradient in the obtained values is quite significant. This is due to the relatively low values observed at the top part of the specimens. Clearly this part undergoes a significantly lower level of compaction compared to deeper parts of the column. Self-compacting concrete flow depends on yield stress and the plastic viscosity of the mixture and flow starts when the self-weight of the material applies enough pressure to overcome the yield stress. Once flow initiates the velocity of the flow depends on the plastic viscosity. There are combinations of these two parameters that lead to poor compaction at the top

part where the self-weight pressure is low. On the other hand, as the depth increases subsequently the compaction becomes better leading to considerably improved strength.

5. Conclusions

This study has validated a new conceptual approach for the characterization of the interface between concrete and steel reinforcement for both SCC and NVC. The objective of the study was to correlate visually recorded defects at the bar-concrete interfaces with basic mixture properties and the position of the bar coupon along the height of the member (top, middle, bottom). The results demonstrated that the proposed methodology can reliably assess the potential for macropore concentration under horizontally laid steel bars. The method gives a clear representation of the network of macropores around reinforcing bars placed orthogonally to the casting direction. Besides being relatively inexpensive and easy to implement, the proposed approach can also identify rapidly the available conditions for bar-concrete interlocking and development of reinforcement, much faster than other common methods, such as pull-out tests. The reason for this is that preparation of a typical specimen requires about 30 minutes, including the bisecting procedure, to be analyzed through imaging.

Self-compacting mixtures were found to be more robust, showing better potential for a good mechanical interlock between steel and concrete. Top-bar effect has been observed only in extreme cases of SCC, where either the mixture was close to segregation (SCC-1) or it did not have the adequate flowability to fill successfully a column-type mold (SCC-2). In normal vibrated concretes, reduced cohesion at the top bar was observed for all mixtures with slump values higher than 150 mm. Moreover, experimental data showed that there is a correlation between viscosity and pore fraction, and between viscosity and total number of pores counted in SCCs. Increasing the relative viscosity of SCCs above 1500 Ns, results in larger pore fraction values, whereas in NVC the phenomenon is reversed owing to the required mechanical vibration for compaction. Controlling viscosity in SCCs to reach an optimum value would result in homogenization of the pore distribution under the bars along the height of a specimen. This would not only eliminate the possibility of top-bar effect, but would also secure an even distribution of macropores,

regardless of the height at which the reinforcing bar was cast. Viscosity modification achieved by using fine fillers or cement replacement materials (such as silica fume in this study) is a more effective way to eliminate defects at the top bar contact area. The use of these materials additionally improves the entire pore network of concrete (including capillary and interlayer pores), thus resulting in a denser and hence more durable material.

6. Acknowledgements

The authors would like to acknowledge financial support from the University of Cyprus (UCY). They would also like to thank the technical personnel of the UCY Building Materials Laboratory for their valuable assistance towards the completion of the experimental work.

Compliance with Ethical Standards:

Funding: This study was funded by University of Cyprus through the internal development schemes. Conflict of Interest: The authors declare that they have no conflict of interest.

7. References

1. Balázs G, Cairns J, Eligehausen R, et al (2014) Bond and anchorage of embedded reinforcement: Background to the fib Model Code for Concrete Structures 2010
2. Yerlici VA, Ozturan T (2000) Factors Affecting Anchorage Bond Strength in HPC. ACI Struct J 97:499–507
3. Chan Y-W, Chen Y-S, Liu Y-S (2003) Effect of Consolidation on Bond of Reinforcement in Concrete of Different Workabilities. Mater J 100:. https://doi.org/10.14359/12667
4. Chan Y-W, Chen Y-S, Liu Y-S (2003) Development of bond strength of reinforcement steel in self-consolidating concrete
5. Barie B. Brettmann and Rex C. Donahey DD (1986) Bond of Reinforcement to Superplasticized Concrete. J Proc 83:. https://doi.org/10.14359/1743
6. Valcuende M, Parra C (2009) Bond behaviour of reinforcement in self-compacting concretes. Constr Build Mater 23:162–170. https://doi.org/10.1016/j.conbuildmat.2008.01.007
7. Zhu W, Sonebi M, Bartos PJM (2004) Bond and interfacial properties of reinforcement in self-compacting concrete. Mater Struct Constr 37:442–448. https://doi.org/10.1617/14012

8. Castel A, Vidal T, Viriyametanont K, François R (2006) Effect of Reinforcing Bar Orientation and Location on Bond with Self-Consolidating Concrete. Struct J 103:559–567. https://doi.org/10.14359/16432
9. Ponmalar S (2018) Bond Behaviour of Self-Compacting Concrete. J Civ Eng 99–105
10. EFNARC (2005) The European Guidelines for Self-Compacting Concrete
11. EN206 - Part I (2004) EN206 - Part I. Concrete: Specification, Performance, Production and Conformity
12. Khayat K, Schutter G De (2014) Mechanical Properties of Self-Compacting Concrete: State of the Art Report of the RILEM Technical Committee 228-MPS on Mechanical Properties of Self Compacting Concrete
13. Shahidan S, Tayeh BA, Jamaludin AA, et al (2017) Physical and mechanical properties of self-compacting concrete containing superplasticizer and metakaolin. IOP Conf Ser Mater Sci Eng 271:012004. https://doi.org/10.1088/1757-899X/271/1/012004
14. Khayat K, Guizani Z (1997) Use of viscosity-modifying admixture to enhance stability of fluid concrete
15. Trezos KG, Sfikas IP, Palmos MS, Sotiropoulou EK (2010) Top-Bar Effect in Self-Compacting Concrete Elements BT - Design, Production and Placement of Self-Consolidating Concrete. In: Khayat KH, Feys D (eds). Springer Netherlands, Dordrecht, pp 355–366
16. Reza Esfahani M, Lachemi M, Reza Kianoush M (2008) Top-bar effect of steel bars in self-consolidating concrete (SCC). Cem Concr Compos 30:52–60. https://doi.org/10.1016/j.cemconcomp.2007.05.012
17. EN 1992-1-1 (1999) Eurocode-2 Design of Concrete Structures (EN 1992-1-1). CEN, Brussels
18. Desnerck P, De Schutter G, Taerwe L (2012) Influence of bar diameter and placement on top-bar effect in self-compacting concrete. Bond Concr 2012 735–742
19. ACI 318 (2014) Building Code Requirements for Concrete Thin Shells and Commentary
20. Khayat KH (1998) Use of Viscosity-Modifying Admixture to Reduce Top- Bar Effect of Anchored Bars Cast with Fluid Concrete. Mater J 95:. https://doi.org/10.14359/361
21. Leemann A, Münch B, Gasser P, Holzer L (2006) Influence of compaction on the interfacial transition zone and the permeability of concrete. Cem Concr Res 36:1425–1433. https://doi.org/10.1016/j.cemconres.2006.02.010
22. Day RL, Marsh BK (1988) Measurement of porosity in blended cement pastes. Cem Concr Res 18:63–73. https://doi.org/10.1016/0008-8846(88)90122-6
23. Ulrik Nilsen A, Monteiro PJM (1993) Concrete: A three phase material. Cem Concr Res 23:147–151. https://doi.org/10.1016/0008-8846(93)90145-Y
24. Bentur A, Diamond S, Mindess S (1985) Cracking processes in steel fiber reinforced cement paste. Cem Concr Res 15:331–342. https://doi.org/10.1016/0008-8846(85)90045-6
25. Soylev TA, François R (2003) Quality of steel-concrete interface and corrosion of reinforcing steel. Cem Concr Res 33:1407–1415. https://doi.org/10.1016/S0008-8846(03)00087-5
26. Winslow D, Liu D (1990) The pore structure of paste in concrete. Cem Concr Res 20:227–235. https://doi.org/10.1016/0008-8846(90)90075-9
27. Neville AM (2002) Properties of Concrete. Pearson Education Limited
28. EN 12350-8 (2010) Testing fresh concrete. Self-compacting concrete. Slump-flow test
29. EN 12350-2 (2009) Testing fresh concrete. Slump-test. 5–8
30. Nemati KM (2001) Analysis of micromechanical behavior of concrete by stereological methods.

Proc First Int Conf Concr Dev C D 1 34:486–494

31. Mouret M, Ringot E (2001) Image analysis: a tool for the characterization of hydration of cement in concrete-metrological aspects of magnification on measurement. Cem Concr Compos 23:201–206
32. Dequiedt AS, Coster M, Chermant L, Chermant JL (2001) Study of phase dispersion in concrete by image analysis. Cem Concr Compos 23:215–226. https://doi.org/10.1016/S0958-9465(00)00060-3
33. Soroushian P, Elzafraney M, Nossoni A (2003) Specimen preparation and image processing and analysis techniques for automated quantification of concrete microcracks and voids. Cem Concr Res 33:1949–1962. https://doi.org/10.1016/S0008-8846(03)00219-9
34. Soroushian P, Elzafraney M (2005) Morphological operations, planar mathematical formulations, and stereological interpretations for automated image analysis of concrete microstructure. Cem Concr Compos 27:823–833. https://doi.org/10.1016/j.cemconcomp.2004.07.008
35. Sumanasooriya MS, Neithalath N (2009) Stereology and morphology based pore structure descriptors of Enhanced Porosity (Pervious) Conretes. ACI Mater J 106:429–438
36. Abell AB, Willis KL, Lange DA (1999) Mercury intrusion porosimetry and image analysis of cement-based materials. J Colloid Interface Sci 211:39–44. https://doi.org/10.1006/jcis.1998.5986
37. Garboczi EJ, Bentz DP, Martys NS (1999) 1. Digital Images and Computer Modeling. In: Wong PBT-EM in the PS (ed) Methods in the Physics of Porous Media. Academic Press, pp 1–41
38. Coster M, Chermant J-L (2001) Image analysis and mathematical morphology for civil engineering materials. Cem Concr Compos 23:133–151. https://doi.org/10.1016/S0958-9465(00)00058-5
39. Okamura H (1996) Self-Compacting High-Performance Concrete. Concr Int
40. Petrou MF, Harries KA, Gadala-Maria F, Kolli VG (2000) A unique experimental method for monitoring aggregate settlement in concrete. Cem Concr Res 30:809–816. https://doi.org/https://doi.org/10.1016/S0008-8846(00)00223-4
41. Keske SD, Barnes RW, Schindler AK, et al (2015) Self-Consolidating Concrete for Prestressed Applications — Phase I : Girder Fabrication and Pre-Erection Performance
42. Hoshino M (1988) Relation Between Bleeding, Coarse Aggregate, and Specimen Height of Concrete. Mater J 86:. https://doi.org/10.14359/2252